Effect of triple-phase contact line on contact angle hysteresis

YU Yang[1*], WU Qun[1], ZHANG Kai[2] & JI BaoHua[1*]

[1] *Biomechanics and Biomaterials Laboratory, Department of Applied Mechanics, School of Aerospace Engineering, Beijing Institute of Technology, Beijing 100081, China;*
[2] *Department of Engineering Mechanics, Tsinghua University, Beijing 100084, China*

Recent studies have shown that the triple-phase contact line has critical effect on the contact angle hysteresis of surfaces. In this study, patterned surfaces with various surface structures of different area fractions were prepared by electron etching on a silicon wafer. The advancing angle, receding angle and hysteresis angle of these surfaces were measured. Our experimental results showed that while the geometry of microstructure and contact line have a minor effect on the advancing angle, they have a significant effect on the receding angle and thus the hysteresis angle. We have shown that the effect of microstructure and the contact line can be described by a quantitative parameter termed the triple-phase line ratio. The theoretical predictions were in good agreement with our experimental results.

contact angle hysteresis, receding angle, surface microstructure, area fraction, contact line ratio, wetting

PACS number(s): 68.35.Ct, 68.03.Cd, 68.08.De, 68.08.-p, 68.08.Bc

The contact angle hysteresis (CAH) is referred to as the difference between the advancing and the receding contact angles. It is a critical measure of the stickiness of a surface, that is, the resistance to motion experienced by a droplet as it rolls off or detaches from a surface. Studies of CAH, particularly on superhydrophobic surfaces, are critically important for understanding many biological and industrial processes, such as biological wet adhesion [1–3], surface treatment in medical devices and MEMS, microfluidics. Recently, the interest in this field has expanded and much progress has been made [4–19].

Contact angle (θ_Y) is a classic parameter in describing the static wetting property of surfaces. It was firstly expressed on flat surface by Young [20] some 200 years ago as, $\cos\theta_Y = \gamma_{LV}/(\gamma_{SV} - \gamma_{SL})$, where $\gamma_{LV}, \gamma_{SV}, \gamma_{SL}$ are liq-uid-vapor, solid-vapor and solid-liquid interface energy, respectively. For the surfaces with roughness (microstructures), there are two classic models for predicting their apparent contact angle, that is the Wenzel model [21] and the Cassie-Baxter model [22]. The Wenzel model is characterized by fully wetting of solid surface as expressed by $\cos\theta_W = r\cos\theta_Y$, where r is the ratio between the actual surface area and the geometric projection. The Cassie-Baxter model tries to explain the trapping of air between liquid and rough surface as expressed by $\cos\theta_{CB} = f\cos\theta_Y + f - 1$, where f is the area fraction of solid-liquid interface.

Recent studies have shown that only the contact angle is not sufficient for describing dynamic wetting behaviors of surfaces. For example, Johnson and Dettre [4] reported that the apparent contact angle differs from Young's contact angle when the droplet rolls along the surface. They defined the contact angle at the front as the advancing angle (θ_A), the rear as the receding angle (θ_R), and considered the dif-

─────────

*Corresponding author (YU Yang, email: yuyang08@bit.edu.cn; JI BaoHua, email: bhji@bit.edu.cn)

ference as the hysteresis angle ($\Delta\theta$). Experimental results have shown that the hysteresis angle is a critical parameter of dynamic wetting properties.

The sources of CAH can be considered by two classical categories. The first is thermodynamic including surface roughness and surface heterogeneity and the second is kinetic hysteresis including surface orientation, surface deformation, liquid penetration and surface mobility [23]. The surface roughness and surface heterogeneity are two of the most common sources found in nature. Experimental observations have shown with exception to size [5,7,8,17,19, 24] (the characteristic dimension of the roughness), the geometry of the triple-phase line [6,12,13,16] as the most important for surface hysteresis. For example, Gao and McCarthy [24] studied the effects of surface textures on the hysteresis by preparing two kinds of polyester textiles. Others have shown that the discontinuity of the triple-phase line can significantly influence the hysteresis [8]. For understanding the roles of the triple-phase line, mathematic models were proposed. Extrand [9] suggested that the linear fraction of contact line is a key parameter of hysteresis. Researchers have also obtained the relationship among contact angle, advancing angle and receding angle by considering the contact line energy [11]. Choi et al. [17] suggested a parameter named the differential parameter (ϕ_d) into the Cassie-Baxter equation to consider the influence of the contact line. However, the mechanisms of how the contact line influences the CAH are still elusive. In this paper, to reveal the effect of the contact line because of surface roughness of different geometries, a series of surfaces with differing microstructures were prepared and the advancing and receding angle of these surfaces were measured.

Furthermore, a theoretical model considering the effect of the contact line was used for comparison with the measurements of the advancing and receding angles.

1 Materials and methods

1.1 Sample preparation and measurement

The samples of silicon wafers with microstructures are prepared by electron beam etching as shown in Figure 1. The microstructures are differed in shape (square pillars and cylinder pillars), size (5.6–60 μm), distribution (square distribution and hexagonal distribution), and area fraction (0.0625–0.5625). Because silicon is a considered a hydrophilic material, the samples were further coated with Octadecyltricholorosilane (OTS) in order to make the samples show hydrophobicity. The contact angle on flat silicon wafer coated with OTS was $(107.3\pm1)°$.

The contact angle, advancing angle and receding angle were measured by OCA20 Device from Dataphysics (Germany). The droplet used in the measurement was made of deionized water with a volume 8 μL. The contact angle was measured by sessile droplet method, while the advancing and receding angle were measured by the method in which a droplet began to move on a tilted surface and then measuring by computer. Each angle was measured multiple times. The measuring precision of the device is $0.1°$.

We ensured that the droplet on the surface was at the Cassie-Baxter wetting state in our experiments, and the wetting state did not alter significantly during the process of measurement.
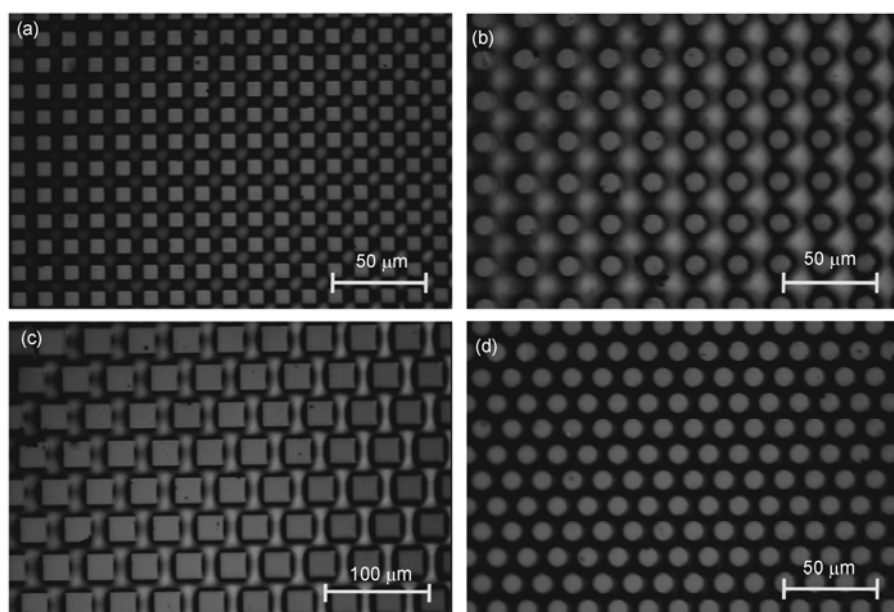

Figure 1 Optical microscopy images of different microstructures of prepared surfaces. (a) Square pillars with square distribution; (b) cylinder pillars with square distribution; (c) square pillars with hexagonal distribution; (d) cylinder pillars with hexagonal distribution.

1.2   Theoretical model

Here we adopted a theoretical model considering the effect of the triple-phase contact line on the CAH. Figures 2(a) and (b) show the illustration of the triple-phase line pins at the side of surface structures. When the water-air interface recedes and contact angle between water and solid reaches receding angle, the triple-phase contact line will break away from the side of the structures, as shown in Figure 2(c). Based on the experimental observations, we proposed that the line ratio of the triple-phase contact line determines the receding angle of the surface. Here we used a one dimensional microstructure pattern, that is the stripe-like microstructure for the derivation. Here we denote the length of the apparent contact line as w, the contact line ratio as g, the ratio of the contact line contacting with solid in yellow to the total length of apparent contact line in red, as illustrated in Figures 2(a) and (b). The length of contact line of solid is now considered gw. Suppose that the three-phase line recedes a distance of Δx (see Figure 2(d)), the changes of energy of solid-vapor, liquid-vapor and solid-liquid interface are given as:

$$\Delta E_{\mathrm{SV}} = \gamma_{\mathrm{SV}} gw \Delta x, \tag{1}$$

$$\Delta E_{\mathrm{LV}} = -\gamma_{\mathrm{LV}} w \Delta x \cos \theta_{\mathrm{R}} - \gamma_{\mathrm{LV}} (1-g) w \Delta x, \tag{2}$$

$$\Delta E_{\mathrm{SL}} = -\gamma_{\mathrm{SL}} gw \Delta x. \tag{3}$$

According to the balance of energy, we have

$$\Delta E_{\mathrm{LV}} + \Delta E_{\mathrm{SL}} + \Delta E_{\mathrm{SV}} = 0. \tag{4}$$

Note that here we adopt the consistent ideas as that of the derivation of Young's Equation and the Cassie-Baxter model in our derivation. That is, the droplet has constant receding and advancing angle with the solid surface during its motion. Thus, the change of surface energy being zero is equivalent to the minimization of the surface energy. From eq. (1) to eq. (4) and Young's equation we can derive the receding angle in terms of the triple-phase line ratio as:

$$\cos \theta_{\mathrm{R}} = g \frac{\gamma_{\mathrm{SV}} - \gamma_{\mathrm{SL}}}{\gamma_{\mathrm{LV}}} + g - 1 = g \cos \theta_{\mathrm{Y}} + g - 1. \tag{5}$$

We extended our derivation of receding angle and calculation of contact line ratio of the one dimensional straight contact line to the curved contact line, which is given in Table 1 for typical surface structures.
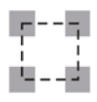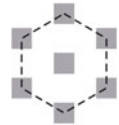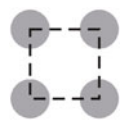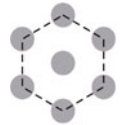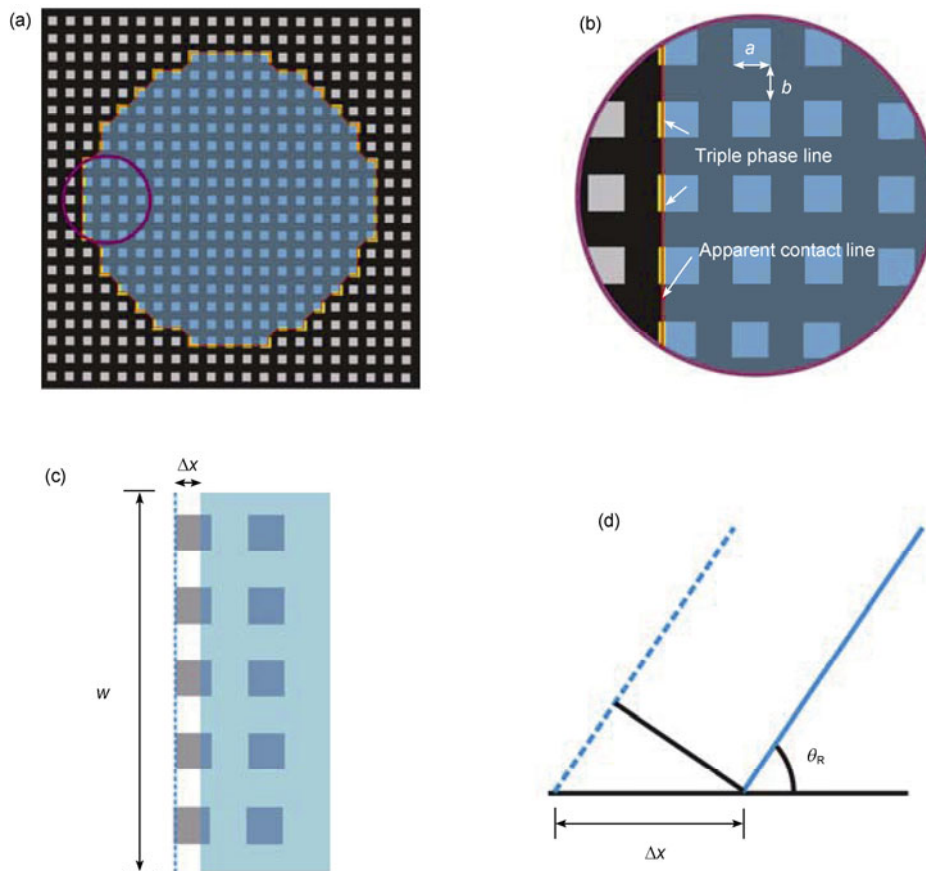

Figure 2   (Color online) Schematic illustration of the theoretical model for receding angle considering the triple-phase line ratio. (a) A droplet sitting on the surface with microstructure; (b) a magnified image of the triple-phase contact line, the triple-phase line and apparent contact line are shown as yellow and orange line, respectively; (c) and (d) illustration of derivation of the theoretical model for receding angle.
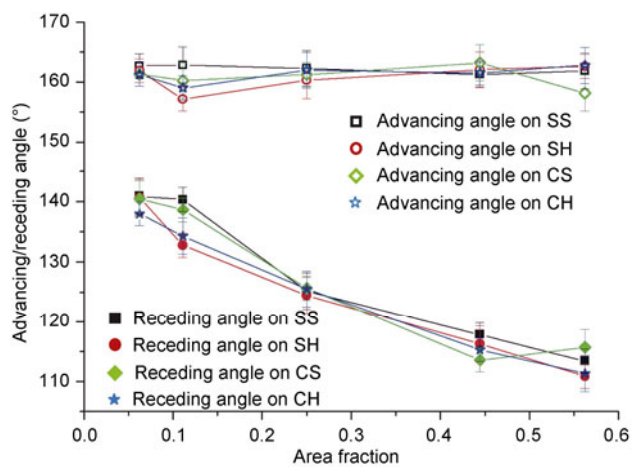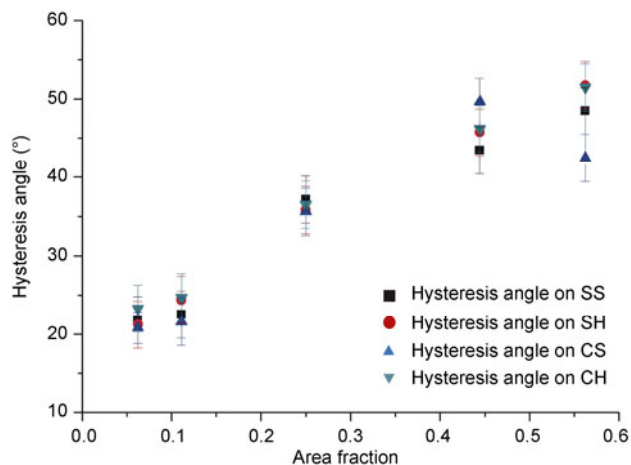
Table 1 Triple-phase line ratio (*g*) relative to area fraction (*f*) of surface structures which were used in our experiments

	Square pillar square distribution	Square pillar hexagonal distribution	Cylinder pillar square distribution	Cylinder pillar hexagonal distribution
Pattern of microstructures				
Triple-phase line ratio (*g*)	$\sqrt{f}$	$\sqrt{\dfrac{24+19\sqrt{3}}{54}f}$	$\sqrt{\dfrac{4}{\pi}f}$	$\sqrt{\dfrac{2\sqrt{3}}{\pi}f}$

2 Results and discussion

The measured values of advancing angle and receding angle of samples of different area fraction, geometry and distribution were shown in Figure 3. As we can see, the area fraction, geometry and distribution only have a slight effect on the advancing angle which changes in a very narrow range from 157° to 163°. In contrast, these parameters have significant effect on the receding angle which alters in a much greaterer range from 100° to 150°. The receding angle decreases with the increase of area fraction of microstructures. In addition, for the same area fraction, different shapes and distributions will produce different receding angles. The hysteresis angles can be calculated from Figure 3 by subtracting advancing angle from the receding angle. As we can see, the hysteresis angle increases with the increase of the area fraction, as shown in Figure 4. Similarly, the hysteresis angle not only depends on the area fraction, but also the geometry and distribution. Therefore, area fraction in itself can not determine the value of the receding angle and hysteresis.

We can also draw the measured values of the receding angle in terms of the triple-phase line ratio, as shown in Figure 5. The black solid curve is for the theoretical predic-

Figure 4 (Color online) Hysteresis angle vs. area fraction of microstructures with different shape and distribution.
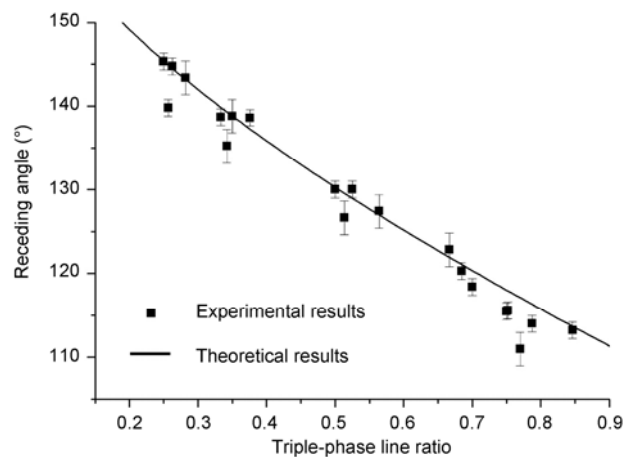
Figure 5 Theoretical predictions of the receding angle at different triple-phase line radio in comparison with the experimental measurements.

tions by eq. (5). The discrete points are measured values. It shows that the experimental results are in good agreement with our theoretical model. In addition, the measured values become less scattered compared with those in Figure 3. This result suggests that the triple-phase line ratio might be a better parameter for describing the CAH of surfaces with microstructures.

The mechanism of above results is that the CAH should

Figure 3 (Color online) Experimental measurements of advancing angle and receding angle vs. area fraction of microstructures with different shape and distribution.

be determined by the triple-phase line ratio. For example, the triple-phase line ratio is different for surface structures by different shapes and distributions even with the same area fraction, as shown in Table 1. As we can see, the triple-phase line ratio of square pillars with square distribution is the smallest among the different surface structures, therefore the receding angle is the largest. In addition, for the same distribution, the triple-phase line ratio of square pillars is smaller than that of the cylinder pillars.

More evidence on the effect of geometry and distribution on the triple-phase line ratio can be found in Figure 6. We can see that the receding angle on the surface with square pillars of square distribution is the largest at same the area fraction. The receding angles on square pillars are higher than those on cylinder pillars. Receding angles on cylinder pillars with hexagonal distribution are higher than those on cylinder pillar with square distribution. All these experimental results are in good agreement with our theoretical predictions based on the triple-phase line ratio.

The theoretical model of receding angle based on the triple-phase line ratio might have important application in design of surface microstructures for controlling the hysteresis of surfaces. It has been shown that the receding angle will increase with the decrease of the triple-phase line ratio from eq. (5). Therefore, decreasing the triple-phase line ratio will decrease the hysteresis. The geometry and distribution can have significant effect on the triple-phase line ratio. For example, the triple-phase line ratio of simple shapes, such as square or circle, are smaller than that of more complex shapes, such as pentagram, flower and hackle-like shapes using the same area fraction. Conversely, the distance between two pillars under square distribution is larger than that under the hexagonal distribution for the same microstructure shape and same area fraction, thus the triple-phase line ratio of square distribution is smaller. Therefore, if one wants to reduce surface hysteresis, one should choose the microstructures with smaller perimeter
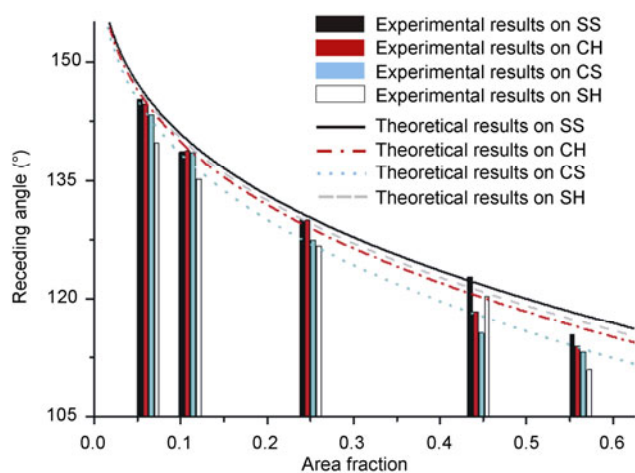
(smaller line ratio) and distribution with larger distances between the structures to further reduce the line ratio.

It can be noted that the advancing angles measured in the experiment alters in a very small range from 157° to 163° although the area fraction of microstructures varied in a large range from 0.0625 to 0.5625. We propose that this phenomenon should be relative to the high apparent contact angle as well as the high area fraction of the surfaces. The underlying mechanisms behind this experimental observation can not be explained using existing theories, particularly at such large area fraction. It was found that even the predictions of contact angle, the Cassie-Baxter model did not agree with the existing experimental measurements of the apparent contact angle. For example, for the area fraction of 0.5625 the prediction of the contact angle by the Cassie-Baxter model should be 127.2°, however, the measured value of the contact angle was as high as (142±2)°.

In addition, it should be noted that although the predictions of our theoretical model based on the triple-phase line ratio are in good agreement with the experimental results, this model currently can not describe the effect of size of the microstructures. More research needs to carried out on improving this model in future work.

3   Conclusion

A series of micro-patterned surfaces with different area fraction, geometry and distribution were prepared by electron beam etching on silicon wafers. The advancing angle, receding angle and hysteresis angle were measured on these microstructured surfaces. The experimental results showed that the advancing angle on those surfaces was not sensitive to the area fraction changing when it was varied within the range from 0.0625 to 0.5625. Conversely, the area fraction had a significant effect on the receding angle. Thus, the larger the area fraction, the smaller the receding angle.

We found that the triple-phase line ratio can be considered a better parameter for predicting the CAH. The area fraction, geometry and distribution of microstructures will all influence the value of triple-phase line ratio. A theoretical model based on the triple-phase line ratio was used for comparison with the experimental measurements. We have shown that the theoretical predictions are in good agreement with the experimental results. In addition, we have shown that the combination of the effects of area fraction, shape and distribution on receding angle could be described by the triple-phase line ratio, which suggests that the triple-phase line ratio might be an appropriate parameter for measurement of CAH of surfaces.

Figure 6   (Color online) Effects of geometry of surface structures on the receding angle.

1   Su Y W, Ji B H, Huang Y G, et al. Concave biological surfaces for strong wet adhesion. Acta Mech Solid Sin, 2009, 22: 593–604

2   Su Y W, Ji B H, Huang Y G, et al. Nature's design of hierarchical superhydrophobic surfaces of a water strider for low adhesion and low-energy dissipation. Langmuir, 2010, 26: 18926–18937

3   Su Y W, He S J, Ji B H, et al. More evidence of the crucial roles of surface superhydrophobicity in free and safe maneuver of water strider. Appl Phys Lett, 2011, 99: 263704

4   Johnson R E, Dettre R H. Contact angle hysteresis (I) Study of an idealized rough surface. Adv Chem Ser, 1964, 43: 112–135

5   Morra M, Occhiello E, Garbassi F. Contact-angle hysteresis in oxygen plasma treated poly (Tetrafluoroethylene). Langmuir, 1989, 5: 872–876

6   Chen W, Fadeev A Y, Hsieh M C, et al. Ultrahydrophobic and ultralyophobic surfaces: Some comments and examples. Langmuir, 1999, 15: 3395–3399

7   Youngblood J P, McCarthy T J. Ultrahydrophobic polymer surfaces prepared by simultaneous ablation of polypropylene and sputtering of poly (tetrafluoroethylene) using radio frequency plasma. Macromolecules, 1999, 32: 6800–6806

8   Oner D, McCarthy T J. Ultrahydrophobic surfaces. Effects of topography length scales on wettability. Langmuir, 2000, 16: 7777–7782

9   Extrand C W. Model for contact angles and hysteresis on rough and ultraphobic surfaces. Langmuir, 2002, 18: 7991–7999

10 Patankar N A. On the modeling of hydrophobic contact angles on rough surfaces. Langmuir, 2003, 19: 1249–1253

11 Tadmor R. Line energy and the relation between advancing, receding, and young contact angles. Langmuir, 2004, 20: 7659–7664

12 Martines E, Seunarine K, Morgan H, et al. Superhydrophobicity and superhydrophilicity of regular nanopatterns. Nano Lett, 2005, 5: 2097–2103

13 Dorrer C, Ruehe J. Advancing and receding motion of droplets on ultrahydrophobic post surfaces. Langmuir, 2006, 22: 7652–7657

14 Yu Y, Zhao Z H, Zheng Q S. Mechanical and superhydrophobic stabilities of two-scale surfacial structure of lotus leaves. Langmuir, 2007, 23: 8212–8216

15 Ng T W, Yu Y, Tan H Y, et al. Capillary well microplate. Appl Phys Lett, 2008, 93: 174105

16 Yeh K Y, Chen L J, Chang J Y. Contact angle hysteresis on regular pillar-like hydrophobic surfaces. Langmuir, 2008, 24: 245–251

17 Choi W, Tuteja A, Mabry J M, et al. A modified Cassie-Baxter relationship to explain contact angle hysteresis and anisotropy on non-wetting textured surfaces. J Colloid Interface Sci, 2009, 339: 208–216

18 Zheng Q S, Yu Y, Feng X Q. The role of adaptive-deformation of water strider leg in its walking on water. J Adhes Sci Technol, 2009, 23: 493–501

19 Su Y W, Ji B H, Zhang K, et al. Nano to micro structural hierarchy is crucial for stable superhydrophobic and water-repellent surfaces. Langmuir, 2010, 26: 4984–4989

20 Young T. An essay on the cohesion of fluids. Philos Trans R Soc London, 1805, 95: 65–87

21 Wenzel R N. Resistance of solid surfaces to wetting by water. Indu Eng Chem, 1936, 28: 988–994

22 Cassie A B D, Baxter S. Wettability of porous surfaces. Trans Faraday Soc, 1944, 40: 546–551

23 Wang B B, Zhao Y P, Yu T. Fabrication of novel superhydrophobic surfaces and droplet bouncing behavior—Part 2: Water droplet impact experiment on superhydrophobic surfaces constructed using ZnO nanoparticles. J Adhes Sci Technol, 2011, 25: 93–108

24 Gao L, McCarthy T J. "Artificial lotus leaf" prepared using a 1945 patent and a commercial textile. Langmuir, 2006, 22: 5998–6000